High-Throughput Mass Spectrometry Imaging of Biological Systems: Current Approaches and Future Directions

Li-Xue Jiang, Manxi Yang, Syeda Nazifa Wali, and Julia Laskin*

Department of Chemistry, Purdue University, West Lafayette, Indiana, 47907, United States

E-mail: jlaskin@purdue.edu

*Corresponding author

Abstract

In the past two decades, the power of mass spectrometry imaging (MSI) for the label free spatial mapping of molecules in biological systems has been substantially enhanced by the development of approaches for imaging with high spatial resolution. With the increase in the spatial resolution, the experimental throughput has become a limiting factor for imaging of large samples with high spatial resolution and 3D imaging of tissues. Several experimental and computational approaches have been recently developed to enhance the throughput of MSI. In this critical review, we provide a succinct summary of the current approaches used to improve the throughput of MSI experiments. These approaches are focused on speeding up sampling, reducing the mass spectrometer acquisition time, and reducing the number of sampling locations. We discuss the rate-determining steps for different MSI methods and future directions in the development of high-throughput MSI techniques.

Keywords: MSI; Throughput; Continuous scanning; Sparse sampling; Multimodal

I. Introduction

Mass spectrometry imaging (MSI) is a powerful label-free technique that provides spatial maps of hundreds of biomolecules with high sensitivity and chemical specificity for biological and clinical research. [1–3] In MSI experiments, mass spectra containing hundreds of peaks are acquired from many locations on the sample thereby generating a chemically-rich snapshot of the molecular state of a biological system. Recent developments in the field are focused on enhancing the spatial resolution and quantitative capabilities of MSI.[4–6] As the spatial resolution increases, the number of pixels increases dramatically thereby decreasing the experimental throughput. For example, imaging of a 10 ×10 mm^2 tissue section with a spatial resolution of 10 μm and pixels distributed evenly across a square grid generates 1 million pixels. When the acquisition time for one pixel is 0.1 s, the total data acquisition time is around 28 h. Similarly, the experimental throughput is one of the major bottlenecks in making 3D MSI experiments more accessible. It follows that the experimental throughput is a key challenge that must be addressed to take full advantage of high resolution and 3D MSI.[7,8]

The acquisition time of MSI experiments is determined by the time required for sampling, mass analysis, and data storage along with time delays associated with hardware and software communication. Although sample preparation and handling are often performed in parallel with data acquisition, substantial improvements in the MSI acquisition rate impose more stringent requirements on the speed of these steps. In this review, we provide a succinct summary of the recent developments in high-throughput MSI of biological samples. We discuss the experimental and computational strategies developed to speed up sampling, reduce the mass spectrometer acquisition time, reduce the number of sampling locations, and automate sample loading. A description of the ionization methods and data analysis approaches used in MSI is outside of the scope of this review. We refer readers to several review articles on these topics.[9–11].

2. Sampling time for each pixel

Two types of sampling methods illustrated in **Figure 1** are used in MSI: ‘microprobe’ and ‘microscope’ modes. The microprobe mode is the most widely used sampling approach in MSI. In the microprobe mode, sampling is performed from one pixel at a time generating the corresponding mass spectrum for each pixel. In contrast, in the microscope mode, MSI works like an optical microscope and multiple pixels are analyzed in each sampling event. In this process, the sample position information is retained using specially-designed ion optics.[12]

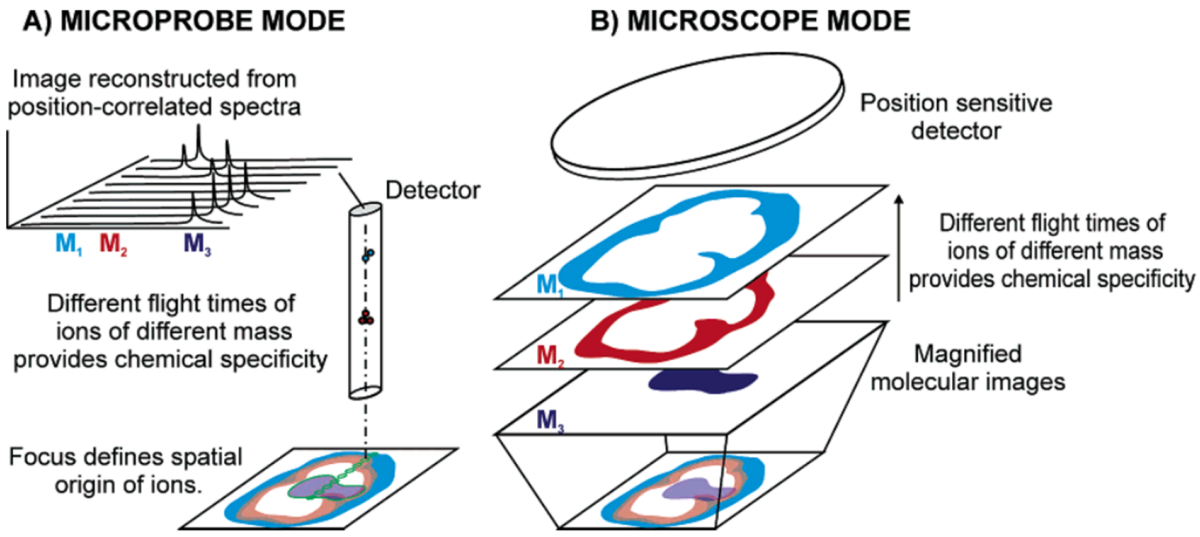

Figure 1. Schematics of the two different approaches to macromolecular imaging mass spectrometry. Microprobe mode imaging (A) collects mass spectra from an array of designated positions to reconstruct a molecular image after completion of the experiment. In microscope imaging (B), magnified images of the ion distributions are directly acquired using a two-dimensional detector. Reprinted from Ref. [13] with permission from ACS.

2.1 Microprobe mode

In the microprobe mode, sampling is performed either by analyzing discrete locations (pointwise or spot-by-spot sampling) or by continuously scanning the analysis probe across the sample (line-wise or continuous scanning mode).[14,15] Pointwise acquisition is commonly used in experiments that generate ions using either laser pulses or pulsed primary ion beams. These include laser desorption-based techniques such as matrix assisted laser desorption ionization (MALDI), laser ablation-based ionization techniques such as laser ablation electrospray ionization (LAESI), secondary ion mass spectrometry (SIMS), and related approaches.[16] Meanwhile, continuous scanning mode is ideally suited for MSI experiments that rely on continuous ionization sources including desorption electrospray ionization (DESI), nanospray desorption electrospray ionization (nano-DESI), liquid microjunction surface sampling probe (LMJ-SSP), and related techniques.[17]

2.1.1 Spot-by-spot scanning mode

In spot-by-spot scanning mode, the stage holding the sample is moved in discrete steps and a set number of laser shots are fired in each step when the stage is stopped.[18] Early MALDI-MSI experiments used low repetition rate lasers (10-20 Hz) and acquired 20-100 laser shots per pixel to improve signal intensity [14] In these experiments, the experimental throughput was mainly determined by the repetition rate of the laser. To increase the experimental throughput, solid state

Nd:YAG lasers operating at >5 kHz were adopted in MALDI MSI, which enabled acquisition rates of around 4 pixels/s.[20] Although, higher repetition rate lasers are available, best performance has been achieved using 5-10 kHz systems. [21] These developments have addressed one of the bottlenecks in high-throughput MALDI MSI, which is no longer limited by the repetition rate of a laser. Another limitation is related to the time it takes for the stage to move between adjacent sampling locations. [18] Depending on the type of the stage and distance between pixels, this time ranges from 20 ms to more than 100 ms. [22,23] The throughput of the spot-by-spot scanning mode is usually less than 10 pixels/s due to time delays associated with stage movement between pixels. [24]

To reduce the translation time between adjacent sampling locations, a laser beam scanning mode has been developed for high-throughput MALDI MSI. [23] In this mode, the sample stage does not move, but the laser beam position is scanned to enable sampling from different locations as shown in **Figure 2**. Laser beam scanning is achieved by a fast-rotating optical mirror, which can precisely move the laser beam between adjacent sampling locations in less than 1 ms. This approach has been used to image small samples at a rate of 147 pixels/s. [24] The high throughput was achieved using a 10 μm pixel size, 5 kHz laser, 10 laser shots per pixel, and improved pulser electronics. In this experiment, the pixel-to-pixel translation time was about 2 ms and data processing/storage time was approximately 3 ms per pixel. With these improvements, a 1.0 × 1.3 mm^2 spheroid sample was imaged in 100 s with a spatial resolution of 10 μm, as shown in **Figure 2**. One limitation of the laser scanning approach is that the laser beam scan range is limited to <1.5 mm by the geometry of the extraction region of MALDI time-of-flight mass spectrometry (TOF-MS) instruments. Thus, a combination of sample stage translation and laser beam scanning is used for large samples. [23] The acquisition rate of 15 pixels/s has been achieved for a 1 cm^2 square sample. It follows that laser beam scanning is ideally suited for the high-throughput imaging of small samples and other strategies must be adopted for larger samples to reduce the time associated with sample stage translation.

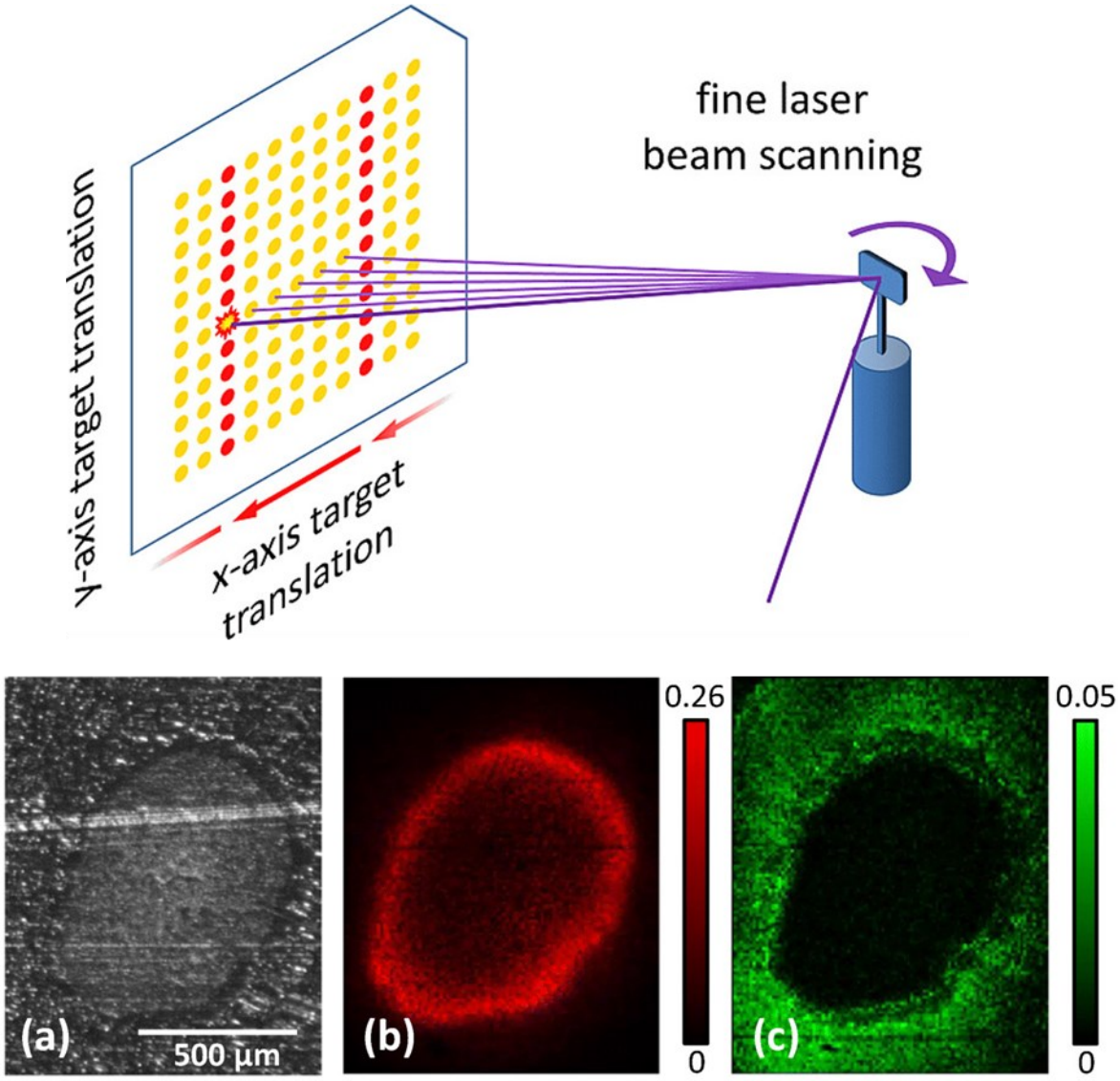

Figure 2. Top: Schematic diagram of the MALDI source used for laser scanning mode. Reprinted from Ref. [23] with permission under the ACS AuthorChoice License. Bottom: Images of one spheroid with a diameter 0.8 mm. (a) Photograph and ion images of (b) cholesterol fragment $[M-H_2O+H]^+$ and (c) perifosine. The sample size is 1.0 × 1.3 mm^2 and the spatial resolution is 10 µm. The total acquisition time is around 100 s with a speed of 130 pixel/s. Adapted from Ref. [24] with permission from ACS.

2.1.2 Continuous scanning mode

2.1.2.1 MALDI-MSI

A continuous scanning mode also referred to as continuous laser raster sampling has been developed to address the slow stage translation that limits the throughput of pointwise MALDI MSI. [15,18,25] In this approach, the laser is fired as the sample stage is scanned at a constant

velocity. Mass spectral data are acquired in lines at the acquisition rate of a mass spectrometer. Using the continuous scanning mode and a high repetition rate laser, the average acquisition rate of 30 pixels/s was achieved in MALDI-MSI experiments.[25] The experiment was performed using the laser repetition rate of 3 kHz and 60 laser shots for each pixel. A substantial increase in the signal intensity was observed at the continuous scanning mode and attributed to oversampling that becomes more severe at slow scan rates. Oversampling originates from the overlap between the areas sampled by adjacent laser shots, which is controlled by the velocity of the sample stage, spot size, and repetition rate of the laser. To address this problem, a galvo mirror system is used to redirect the laser to keep a defined number of laser shots on the same location while the sample stage is continuously moving. [26]

2.1.2.2 DESI-MSI

Liquid extraction-based ambient ionization techniques have gained popularity in MSI experiments.[17] In DESI, the most widely used ambient ionization technique, sample surface is bombarded by charged solvent microdroplets generating secondary droplets that contain analyte molecules.[27] Subsequent desolvation of the secondary droplets generates analyte ions. In MSI experiments, mass spectra are acquired while the sample is moved in lines under the DESI sprayer. Similar to other ambient ionization techniques, DESI requires little to no sample pretreatment. Tissue sections can be analyzed directly after sectioning, which reduces the sample handling time. Typical spatial resolution obtained in DESI MSI is 50-200 μm, the most common scan velocity is ~100 μm/s, and the lateral spacing between lines is adjusted to maintain the desired pixel size.[11] A robust DESI sprayer was developed to further improve the spatial resolution, sensitivity, and throughput of DESI-MSI.[28] In that study, the acquisition rate was ~30 pixels/s when the stage moved at a speed of 1.5 mm/s with a pixel size of 50 μm. Further improvement in the throughput may be achieved using a faster mass spectrometer.

2.1.2.3 Nano-DESI-MSI

Nano-DESI MSI is an emerging ambient MSI technique, in which analytes are extracted into a liquid bridge formed between two fused silica capillaries assembled at an angle of ~90-120° (**Figure 3A**).[29,30] The extracted analytes are transferred to a mass spectrometer and ionized by electrospray ionization. MSI data acquisition is performed using a continuous scan mode with a typical scan rate of 5–50 μm/s. A first high throughput nano-DESI MSI experiment was performed using a scan rate of 0.2 mm/s and a spatial resolution of 150 μm.[31] This approach enabled 3D imaging of a relatively small (<2 mm in diameter) mouse uterine tissue in 4.5 h. Lower scan rates of ~20 μm/s are typically used in high spatial resolution nano-DESI MSI experiments to maintain a stable liquid bridge on the sample surface and match the acquisition rate of a mass spectrometer. [32]

Recently, an integrated microfluidic probe (iMFP) has been developed for nano-DESI MSI. [33,34]The iMFP contains a sampling port formed by two microfluidic channels: one channel

transfers the extraction solvent to the sample surface and the other channel transfers the extracted analytes to a finely polished tip for electrospray ionization (**Figure 3B**). The robustness of the iMFP enabled high-throughput imaging using a scan rate of up to 0.4 mm/s and a spatial resolution of 25-30 μm. [34] Both the design of the iMFP and solvent flow rate were adjusted to ensure the stability of the liquid bridge during the experiment and eliminate carryover, which becomes more important at high scan rates. The mouse brain imaging data obtained at scan rates ranging from 0.04 to 0.4 mm/s using the high-throughput iMFP are shown in **Figure 3**. Line profiles of PC 34:1 shown in **Figure 3C** obtained at different scan rates indicate comparable signal stability and sensitivity, respectively, across all the scan rates. Meanwhile, representative ion images shown in **Figure 3D** demonstrate good correspondence between the spatial localization patterns of lipid species acquired at different scan rates. At the highest scan rate, the total acquisition time of 21.7 min was achieved for a mouse brain tissue sample at no expense to the quality of the MSI data. For the scan rate of 0.4 mm/s, the spatial resolution is limited by the acquisition rate of a mass spectrometer. In order to achieve a spatial resolution of 10 μm at this scan rate, the acquisition rate must be greater than 40 Hz.

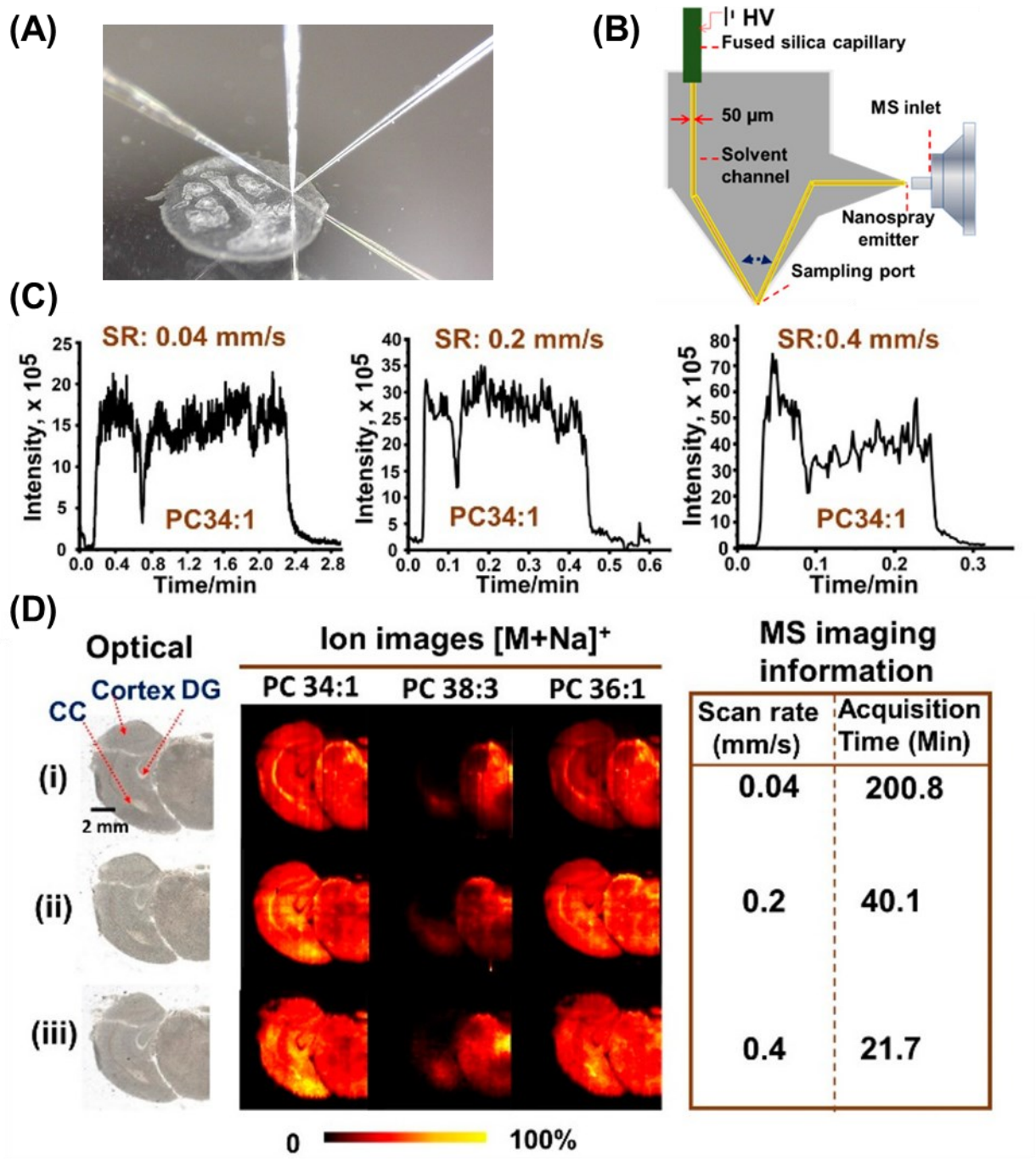

Figure 3. (A) A photograph of a capillary-based nano-DESI probe placed onto a tissue sample. (B) A schematic diagram of the iMFP. (C) Representative line profiles of PC 34:1 (*m*/*z* 782.568) across a mouse brain tissue section at different scan rates. (D) Optical images of tissue sections used at (i) 0.04, (ii) 0.2, and (iii) 0.4 mm/s scan rates. Representative positive mode ion images obtained for $[M + Na]^+$ ions of PC 34:1, PC 38:3, and PC 36:1 along with image acquisition times. The following regions are labeled in the optical image: cortex, dentate gyrus (DG), and corpus callosum (CC). Scale bar: 2 mm. The intensity scale: black (low); yellow (high). Adapted from Ref. [34] with permission from ACS.

2.2 Microscope mode

Microscope mode MSI imaging addresses both the spatial resolution and experimental throughput challenges of microprobe approaches discussed earlier. In this mode, molecules desorbed from different locations on the sample are simultaneously analyzed by projecting an ion beam onto a position-sensitive detector, as shown in **Figure 1**.[13] Ion position information is preserved and magnified 10-20 times using specially designed ion optics. The spatial resolution of microscope MSI is limited by aberrations caused by the ion optics and the capabilities of the position-sensitive detector.[35,36] A spatial resolution of 1-10 μm was obtained for a field diameter of several hundreds of μm.[13,37] Imaging of a larger sample was performed by stitching several fields-of-view. In early experiments, only one *m/z* could be detected in a microscope MSI due to limitations of position-sensitive detectors composed of a phosphor screen and a charge-coupled device camera. Although these detectors are robust, the long luminescence decay time of the phosphor screen dramatically reduces the mass resolution of TOF instruments. [36] As a result, only one *m/z* can be used per experiment. To overcome this limitation, novel position-sensitive detectors including delay-line detectors, Medipix series detectors, and pixel imaging mass spectrometry (PImMS) sensors have been developed for MSI. [38]

It has been suggested that the microscope mode may be used to improve the throughput of MSI experiments by several orders of magnitude. [13] Preserving the initial position information of ions during analysis is key design consideration for microscope MSI instruments. To preserve the position information, ions must be extracted immediately after ionization. Thus, delayed extraction typically used to improve the mass resolution of TOF-MS cannot be directly used in these systems. To improve the mass resolution of microscope MSI, a post-extraction differential acceleration approach has been developed to compensate for the initial velocity distribution of ions.[39] In this approach, ions are still extracted immediately after ionization to preserve image quality. However, the extraction voltage is increased after a short delay while ions are still traveling in the extraction region. The increase in the extraction voltage helps compensate for the velocity dispersion. Using this approach, a mass resolution of 1,450 has been achieved on a linear TOF with a flight length of 790 mm. This presents a substantial improvement in comparison with a mass resolution of 60 obtained using a conventional single-pulse extraction. The mass resolution was further improved to 8,100 by using a reflectron TOF in one ion microscope.[40] A mass resolution of 10,000 has been reported in a projection-type imaging mass spectrometer using a multi-turn TOF with specially-designed ion optics and post-extraction differential acceleration. [37] Using this system, imaging of a 16 × 4 mm^2 marine fish section with a spatial resolution of 2 μm was performed in about 12 h using 132 fields of view. This experiment generated 18.5 × 10^6 pixels and the effective acquisition speed was 428 pixels/s. The throughput of these experiments is limited by the acquisition speed of delay-line detectors, which can only detect a limited number of ions at the same time. In comparison, a Timepix3 detector from Medipix series coupled with a continuously

sampling SIMS-based microscope MSI enables data acquisition at 15,500 pixels/s with a pixel size of 0.5 μm. [41]

3 Mass spectrometer acquisition time

3.1 MS1

With the improvements in the sampling speed, the acquisition speed of a mass spectrometer becomes one of the key factors that limits the throughput of the microprobe mode MSI. In TOF-MS, the minimum time for acquiring one mass spectrum determined by the flight time of the heaviest ions, which is typically around 200 μs corresponding to a 5000 Hz data acquisition rate. An average or sum of at least 10 mass spectra is often used to improve the sensitivity, which reduces the throughput to about 500 pixels/s. This high throughput has been achieved using a high-sensitivity MALDI-TOF MSI platform operated in the continuous laser raster mode with a 5 kHz laser and 10 laser shots per pixel, which reduced the acquisition time per pixel to 2 ms. [42] The sample stage velocity was 5 mm/s for imaging with 10 μm pixel size, for which the transition time between pixels was also 2 ms. The high sensitivity is achieved using a linear axial TOF and a specially-designed ion optics system, which provides sufficient sensitivity using only 10 laser shots per pixel. In addition, a high-rate detector system which can acquire, process, and save spectra at 1000 Hz has been developed to support the high throughput acquisition. The effective imaging speed of this system is about 300 pixels/s, which is limited by the data processing and storage time. It should be noted that high throughput MSI experiments with an acquisition rate of greater than 50 pixels/s are typically performed on axial TOF instruments. For orthogonal TOF systems, the acquisition rate is usually less than 50 Hz. For example, the throughput of ~20 pixels/s was obtained using a MALDI QTOF instrument equipped with a 10 kHz laser system and operated in the continuous scan mode.[43] The acquisition rate of the orthogonal TOF may be improved by adding a fast ion storage device in front of the TOF or performing multiple ion extractions into the flight tube.[44,45]

Orbitraps and Fourier transform ion cyclotron resonance (FT-ICR) MS instruments provide high mass resolving power and mass accuracy, which facilitate the identification of extracted analytes based on the accurate *m/z* measurement.[46] Mass resolving power of these instruments is dependent on the length of the time-domain (transient) signal. For a mass resolution of $m/\Delta m$>500,000, the transient time is typically 500 ms or longer, which corresponds to the data acquisition rate of less than 2 pixels/s.[47–49] A subspace approach has been developed to improve the throughput of MSI experiments on FT-ICR platforms without a substantial loss in mass resolution. [50,51] In this approach illustrated in **Figure 4**, a subset of long transients is acquired from several locations on the sample (10%). Long transients are decomposed into a set of basis transient signals that are subsequently used for data reconstruction. Short transients are acquired for the remaining pixels. Subsequent fitting of short transients using a linear combination of basis

transients is used to reconstruct high-resolution mass spectra in each pixel of the image. This subspace approach provides a 10-fold improvement in throughput while maintaining high mass resolution of the spectral data.

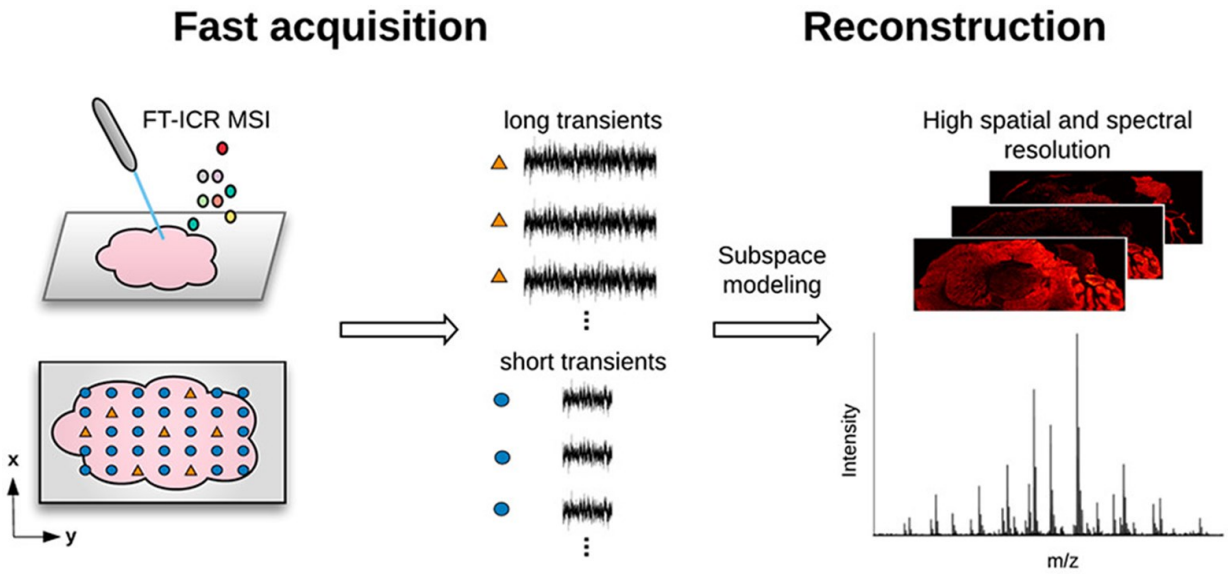

Figure 4. Subspace-based imaging for FT-ICR MSI. The subspace model starts with randomly sampling 10% of the transients with the long transient duration (0.734 s) to construct the transient set. The left pixels are acquired by shorter transient time (0.11s). The shorter transient time data are reconstructed to long transient data based on subspace method. This acquisition and reconstruction strategy can improve the data acquisition efficiency without compromising the spectral resolution and mass accuracy. Reprinted from Ref. [50] with permission from ACS.

3.2 MS2

MS/MS imaging is a powerful technique for the simultaneous identification and spatial localization of isomeric and isobaric compounds, which commonly complicate mass spectral data and introduce ambiguity to data interpretation due to the presence of multiple species at the same *m/z*.[6] Although high-resolution MS analysis may be used to distinguish isobaric compounds, other approaches such as ion mobility separation or MS/MS must be used for the identification of isomeric species. One of the caveats of MS/MS imaging is a relatively low throughput of these experiments when performed in an untargeted manner. A pixel acquisition rate of 13 Hz for one precursor has been achieved on a MALDI TOF/TOF system using the continuous scanning mode.[18] Nano-DESI MSI in MS/MS mode has been used to target 92 precursors with an average acquisition time of 14.7 s for each pixel using a Q-Exactive Orbitrap, which corresponds to about 6 precursors per second. [52] In another study, multiple reaction monitoring (MRM) mode on a DESI-triple quadrupole system was used for mapping of low-abundance lipid molecules in rat brain tissue sections.[53] A dwell time of 0.199 s was used for MRM imaging, which corresponds to the acquisition rate of 5 pixels/s for a single precursor.

Another approach for the high throughput MS/MS acquisition of MSI data involves parallel accumulation serial fragmentation (PASEF) implemented on a trapped ion mobility TOF instrument (timsTOF).[54] In this experiment, ion elution from a trapped ion mobility cell is synchronized with mass selection by a quadrupole mass filter and fragmentation in a collision cell. PASEF mode enables serial fragmentation of multiple precursors at a rate of up to 100 Hz. PASEF mode MALDI-MSI has been used for imaging of 25 precursors in a small pixel (10 μm).[55] This acquisition mode will substantially expand the high throughput capabilities of MS/MS MSI experiments.

4 Sparse sampling

Computational approaches play a critical role in high throughput MSI.[10] Compressed sensing also called sparse sampling is one of the strategies for enhancing the experimental throughput. This approach enables the reconstruction of high-quality imaging data using a fraction of experimentally sampled locations.[56] Based on the method used to determine sampling locations, sparse sampling can be divided into static and dynamic techniques.[57] In static sparse sampling, the sampling locations are determined before the experiment. Typically, 25-50% sampling is used in these experiments, which results a 2-4-fold improvement in throughput.[51,58] Meanwhile, in dynamic sparse sampling, the sampling locations are predicted based on the acquired data. In dynamic sparse sampling, information-rich positions are preferentially sampled, which results in a higher throughput of the MSI experiment. We note that sample heterogeneity may affect the outcome of sparse sampling, especially for dynamic sparse sampling. Multiple *m*/*z* channels were monitored in the process of predicting the sampling position due to the molecular heterogeneity of samples.[59] Although sparse sampling has been widely applied in other imaging modalities [60–62], only a few studies have implemented this approach in MSI .[51,59]

4.1 Static sparse sampling

4.1.1 Uniform and random sparse sampling

In uniform sparse sampling, the sampled locations are uniformly distributed across the entire sample area. A super-resolution reconstruction method has been developed to improve the spatial resolution of undersampled ion images, which simulates the uniform sparse sampling method. [58] In that study, low-resolution MSI data were generated by merging four pixels of a high-resolution image into one pixel. Subsequent reconstruction of the low-resolution MSI data generated high-resolution image demonstrating the potential of uniform sparse sampling. Random sparse sampling uses randomly-selected sampling locations. A simulation of random sparse sampling was performed by resampling a fully acquired DESI MSI data set to include half of the pixels and subsequent reconstruction of ion images with high fidelity.[63] The first random sparse sampling experiment was performed on a MALDI FT-MSI system.[51] Good-quality image reconstruction,

which retained most of the spatial features was achieved using 40-60% of sparsely sampled pixels selected at random.

4.1.2 Combining modalities for data-dependent sampling

In data-dependent sampling, only selected regions of interest (ROI) are analyzed by MSI. ROIs are determined based on the results obtained using a fast imaging technique such as optical or infrared microscopy. The ROI position information is subsequently used to guide sampling in MSI experiments. This multimodal guided strategy substantially reduces the analyzed area of the sample, which increases the throughput of MSI. An integrated approach, in which Fourier transform infrared (FTIR) microscopy is used to automatically guide MALDI MSI has been used for imaging of mouse brain tissue sections.[64] In this experiment, an automated segmentation of the FTIR image was used to target dentate gyrus of the hippocampus in MALDI-FTICR-MSI measurement. **Figure 5** shows the concept of the multimodal FTIR-guided MALDI mass spectrometry imaging of a mouse brain tissue section. Fast and non-destructive FTIR imaging was performed to determine the location of dentate gyrus using image segmentation. This position information was transferred to MALDI-MSI system and used as the sampling area. A 97.8% reduction in data acquisition time was achieved in this experiment, which was completed in 25 min instead of 18.3 h required for imaging of the whole tissue section. Other imaging modalities summarized in a recent review may be used to improve the throughput of MSI experiments.[65]

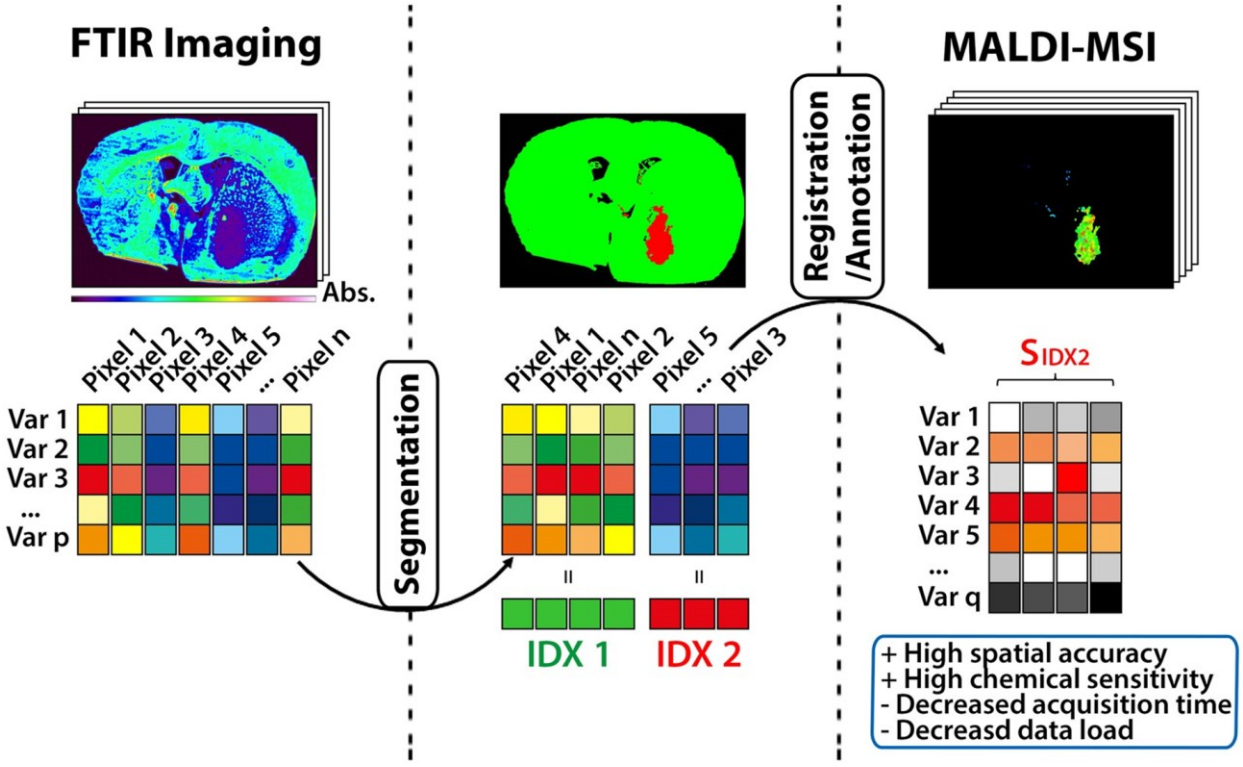

Figure 5. Concept of multimodal FTIR-guided MALDI mass spectrometry imaging. In a two-modality workflow, FTIR imaging is used as the first modality to record a variable (Var) set of p

vibrational bands that represent molecular distribution patterns at a pixel size limit of 6.25 × 6.25 μm^2. By applying segmentation, FTIR spectra of all acquired pixels are separated into a defined number of subgroups based on spectral similarities. The membership of each FTIR pixel to one of the defined groups is expressed by assigning an exclusive index number (IDX). The spatial properties of a segment belonging to a given IDX (S_{IDX}) are automatically registered to the second modality, MALDI-MSI, allowing for a targeted acquisition of a greater number of q mass variables for the region of interest predefined by the FTIR subgroup. FTIR and MS imaging measure different properties of the examined tissue specimen, thus complementing contours of spatial accuracy that exceed MALDI-MSI capabilities with chemically specific mass information while reducing data load and acquisition time. Reprinted from Ref. [64] with the permission from authors.

4.2 Dynamic sparse sampling

A deep learning approach for dynamic sparse sampling (DLADS) has been developed to direct the sampling to molecularly informative locations, which increases the experimental throughput.[59,66] DLADS is initialized by sampling a small number of randomly selected pixels on the sample. Based on these measurements, a deep learning model trained on high-quality MSI data is used to iteratively predict next sampling locations that maximize the entropy metric called the estimated reduction in distortion. A 2.3-fold improvement in the experimental throughput has been achieved using DLADS optimized for the linewise acquisition mode in nano-DESI MSI experiments.[59] As shown in **Figure 6**, full images were reconstructed with high fidelity using 40% of sampled locations across the tissue section. Meanwhile, simulations predict that only 10% sampled pixels are required to obtain high-quality image reconstruction in DLADS MALDI-MSI experiments, which corresponds to a 10-fold improvement in throughput. A better performance of DLADS in the pointwise acquisition mode is attributed to the lack of the line-bounded geometry constraint presenting in DLADS coupled with linewise acquisition mode.

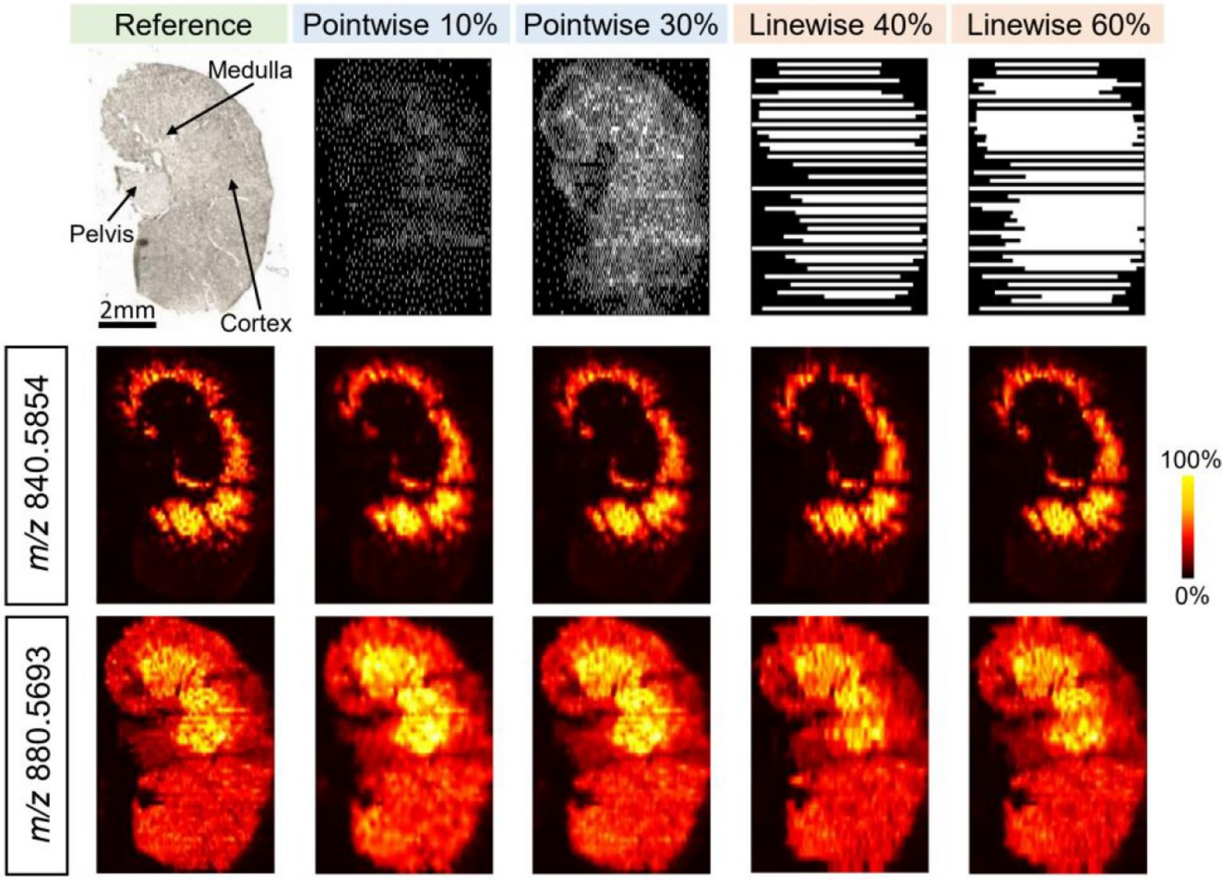

Figure 6. Simulated DLADS dynamic sampling and reconstruction in the pointwise and linewise modes, using a fully measured mouse kidney tissue MSI data. An optical image and ground-truth ion images of *m/z* 840.5854 and *m/z* 880.5693 are shown in the first column. DLADS sampling locations and reconstructed ion images at different simulation conditions are shown in columns 2−5. The results are shown for 10% and 30% sampling in the spot-by-spot mode and 40% and 60% sampling in the continuous line scan mode. Reprinted from Ref. [59] with the permission from authors.

5. Automated sample loading

In current MSI experiments, the acquisition time for imaging of one tissue section with 10 μm spatial resolution is relatively long. However, with the improvement in the experimental throughput, data acquisition time may become comparable to the time required for sample loading into the instrument. Robotic platforms for fully automated MSI experiments may be used to further increase the throughput by minimizing sample loading time. In a proof-of-concept study, an automated MSI platform composed of a sample repository and a robotic sample loading system coupled with a MALDI TOF/TOF instrument has been shown to provide a robust and reproducible performance necessary for clinical applications. [67] Sample degradation during the analysis,

which lasted for 1.5 days was substantially reduced by controlling the humidity and oxygen levels in the sample repository.

6. Conclusions and Outlook

Recent developments in MSI instrumentation and methodology have opened up opportunities for the label-free molecular imaging of biological samples with high chemical specificity, sensitivity, and subcellular spatial resolution. With these developments, the experimental throughput has become a limiting factor for imaging of large samples with high spatial resolution and 3D imaging of tissues. A substantial effort has been dedicated to increasing the throughput of MSI experiments without compromising other performance characteristics. A combination of rapid sampling with continuous scanning of the sample and fast data acquisition has enabled the acquisition rate of more than 300 pixels/s in MALDI-TOF MSI experiments. Meanwhile, the throughput of ambient MSI is limited by the acquisition rate of MS instruments. Reducing the number of sampled locations is another strategy that has been used in high-throughput MSI experiments. One promising approach involves microscope mode MSI, in which ions generated from different locations on the sample are simultaneously analyzed using a specially designed ion optics and position-sensitive detector. In another approach, multiple imaging modalities are combined to identify and direct MSI analysis to selected ROIs on the sample. Meanwhile, computational approaches have been developed to enable sparse sampling in MSI experiments. Both static and dynamic sparse sampling have been used to reduce the number of sampled pixels while providing high-fidelity image reconstruction. These approaches provide an additional throughput enhancement on top of any other developments in both the spot-by-spot and continuous scanning acquisition modes. Collectively, these advances in sampling and acquisition have been used to reduce the analysis time from hours to minutes making the acquisition rate of a mass spectrometer and sample loading the rate limiting steps. Future developments in mass spectrometry instrumentation along with the implementation of automated sample loading platforms will enable new applications of high throughput MSI in biology, drug discovery, and clinical research.

Acknowledgements

The authors acknowledge support from the National Institutes of Health (NIH) Award RF1MH128866 (BICCN) and UH3CA255132 (HuBMAP) along with support from the National Science Foundation (NSF-2108729). Part of our MSI research was supported by the Center for Bioanalytical Metrology, an NSF Industry-University Cooperative Research Center (Grant IIP-1916691).

References

[1] J.G. Swales, G. Hamm, M.R. Clench, R.J.A. Goodwin, Mass spectrometry imaging and its application in pharmaceutical research and development: A concise review, Int J Mass Spectrom. 437 (2019) 99–112. https://doi.org/10.1016/j.ijms.2018.02.007.

[2] B. Spengler, Mass spectrometry imaging of biomolecular information, Anal Chem. 87 (2015) 64–82. https://doi.org/10.1021/ac504543v.

[3] A.R. Buchberger, K. DeLaney, J. Johnson, L. Li, Mass spectrometry imaging: A review of emerging advancements and future insights, Anal Chem. 90 (2018) 240–265. https://doi.org/10.1021/acs.analchem.7b04733.

[4] D. Unsihuay, D.M. Sanchez, J. Laskin, Quantitative Mass Spectrometry Imaging of Biological Systems, Annu Rev Phys Chem. 72 (2020) 307–329. https://doi.org/10.1146/annurev-physchem-061020-053416.

[5] T.C. Baker, J. Han, C.H. Borchers, Recent advancements in matrix-assisted laser desorption/ionization mass spectrometry imaging, Curr Opin Biotechnol. 43 (2017) 62–69. https://doi.org/10.1016/j.copbio.2016.09.003.

[6] C. Zhao, Z. Cai, Three-dimensional quantitative mass spectrometry imaging in complex system: From subcellular to whole organism, Mass Spectrom Rev. 41 (2022) 469–487. https://doi.org/10.1002/MAS.21674.

[7] P.M. Vaysse, R.M.A. Heeren, T. Porta, B. Balluff, Mass spectrometry imaging for clinical research-latest developments, applications, and current limitations, Analyst. 142 (2017) 2690–2712. https://doi.org/10.1039/C7AN00565B.

[8] D.R.N. Vos, S.R. Ellis, B. Balluff, R.M.A. Heeren, Experimental and data analysis considerations for three-dimensional mass spectrometry imaging in biomedical research, Mol Imaging Biol. 23 (2021) 149–159. https://doi.org/10.1007/s11307-020-01541-5.

[9] J. Xue, Y. Bai, H. Liu, Recent advances in ambient mass spectrometry imaging, TrAC - Trends in Analytical Chemistry. 120 (2019) 115659. https://doi.org/10.1016/j.trac.2019.115659.

[10] H. Hu, J. Laskin, Emerging computational methods in mass spectrometry imaging, Advanced Science. (2022) 2203339. https://doi.org/10.1002/advs.202203339.

[11] C. Wu, A.L. Dill, L.S. Eberlin, R.G. Cooks, D.R. Ifa, Mass spectrometry imaging under ambient conditions, Mass Spectrom Rev. 32 (2013) 218–243. https://doi.org/10.1002/MAS.21360.

[12] J.H. Jungmann, R.M.A. Heeren, Emerging technologies in mass spectrometry imaging, J Proteomics. 75 (2012) 5077–5092. https://doi.org/10.1016/J.JPROT.2012.03.022.

[13] S.L. Luxembourg, T.H. Mize, L.A. McDonnell, R.M.A. Heeren, High-spatial resolution mass spectrometric imaging of peptide and protein distributions on a surface, Anal Chem. 76 (2004)

5339–5344.
https://doi.org/10.1021/AC049692Q/ASSET/IMAGES/LARGE/AC049692QF00005.JPEG.

[14] M. Stoeckli, P. Chaurand, D.E. Hallahan, R.M. Caprioli, Imaging mass spectrometry: A new technology for the analysis of protein expression in mammalian tissues, Nat Med. 7 (2001) 493–496. https://doi.org/10.1038/86573.

[15] D.A. Simmons, Improved MALDI-MS imaging performance using continuous laser rastering, Applied Biosystems Technical Note. (2008).

[16] R. Hu, Y. Li, Y. Yang, M. Liu, Mass spectrometry-based strategies for single-cell metabolomics, Mass Spectrom Rev. (2021) 1–28. https://doi.org/10.1002/mas.21704.

[17] J. Laskin, I. Lanekoff, Ambient mass spectrometry imaging using direct liquid extraction techniques, Anal Chem. 88 (2016) 52–73. https://doi.org/10.1021/acs.analchem.5b04188.

[18] B.M. Prentice, C.W. Chumbley, R.M. Caprioli, High-speed MALDI MS/MS imaging mass spectrometry using continuous raster sampling J. Mass Spectrom.. 50 (2015) 703–710. https://doi.org/10.1002/jms.3579.

[19] J. Preisler, P. Hu, T. Rejtar, E. Moskovets, B.L. Karger, Capillary array electrophoresis-MALDI mass spectrometry using a vacuum deposition interface, Anal Chem. 74 (2002) 17–25. https://doi.org/10.1021/AC010692P/ASSET/IMAGES/LARGE/AC010692PF00005.JPEG.

[20] P.J. Trim, M.C. Djidja, S.J. Atkinson, K. Oakes, L.M. Cole, D.M.G. Anderson, P.J. Hart, S. Francese, M.R. Clench, Introduction of a 20 kHz Nd:YVO4 laser into a hybrid quadrupole time-of-flight mass spectrometer for MALDI-MS imaging, Anal Bioanal Chem. 397 (2010) 3409–3419. https://doi.org/10.1007/S00216-010-3874-6.

[21] R.T. Steven, A. Dexter, J. Bunch, Investigating MALDI MSI parameters (Part 2) – On the use of a mechanically shuttered trigger system for improved laser energy stability, Methods. 104 (2016) 111–117. https://doi.org/10.1016/j.ymeth.2016.04.013.

[22] P. Chaurand, K.E. Schriver, R.M. Caprioli, Instrument design and characterization for high resolution MALDI-MS imaging of tissue sections, J. Mass Spectrom. 42 (2007) 476–489. https://doi.org/10.1002/jms.1180.

[23] A. Bednařík, P. Kuba, E. Moskovets, I. Tomalová, P. Krásenský, P. Houška, J. Preisler, Rapid matrix-assisted laser desorption/ionization time-of-flight mass spectrometry imaging with scanning desorption laser beam, Anal Chem. 86 (2014) 982–986. https://doi.org/10.1021/ac402823n.

[24] A. Bednařík, M. Machálková, E. Moskovets, K. Coufalíková, P. Krásenský, P. Houška, J. Kroupa, J. Navrátilová, J. Šmarda, J. Preisler, MALDI MS imaging at acquisition rates exceeding 100 pixels per second, J Am Soc Mass Spectrom. 30 (2019) 289–298. https://doi.org/10.1007/s13361-018-2078-8.

[25] J.M. Spraggins, R.M. Caprioli, High-speed MALDI-TOF imaging mass spectrometry: Rapid ion image acquisition and considerations for next generation instrumentation, J Am Soc Mass Spectrom. 22 (2011) 1022–1031. https://doi.org/10.1007/S13361-011-0121-0/ASSET/IMAGES/MEDIUM/JS8B04044_0006.GIF.

[26] N.O. Potočnik, T. Porta, M. Becker, R.M.A. Heeren, S.R. Ellis, Use of advantageous, volatile matrices enabled by next-generation high-speed matrix-assisted laser desorption/ionization time-of-flight imaging employing a scanning laser beam, Rapid Commun. Mass Spectrom. 29 (2015) 2195–2203. https://doi.org/10.1002/rcm.7379.

[27] Z. Takáts, J.M. Wiseman, B. Gologan, R.G. Cooks, Mass spectrometry sampling under ambient conditions with desorption electrospray ionization, Science (1979). 306 (2004) 471–473. https://doi.org/10.1126/SCIENCE.1104404.

[28] J. Tillner, V. Wu, E.A. Jones, S.D. Pringle, T. Karancsi, A. Dannhorn, K. Veselkov, J.S. McKenzie, Z. Takats, Faster, more reproducible DESI-MS for biological tissue imaging, J Am Soc Mass Spectrom. 28 (2017) 2090–2098. https://doi.org/10.1007/s13361-017-1714-z.

[29] P.J. Roach, J. Laskin, A. Laskin, Nanospray desorption electrospray ionization: An ambient method for liquid-extraction surface sampling in mass spectrometry, Analyst. 135 (2010) 2233–2236. https://doi.org/10.1039/C0AN00312C.

[30] J. Laskin, B.S. Heath, P.J. Roach, L. Cazares, O.J. Semmes, Tissue imaging using nanospray desorption electrospray ionization mass spectrometry, Anal Chem. 84 (2012) 141–148. https://doi.org/10.1021/AC2021322.

[31] I. Lanekoff, K. Burnum-Johnson, M. Thomas, J. Cha, S.K. Dey, P. Yang, M.C. Prieto Conaway, J. Laskin, Three-dimensional imaging of lipids and metabolites in tissues by nanospray desorption electrospray ionization mass spectrometry, Anal Bioanal Chem. 407 (2015) 2063–2071. https://doi.org/10.1007/s00216-014-8174-0.

[32] R. Yin, K.E. Burnum-Johnson, X. Sun, S.K. Dey, J. Laskin, High spatial resolution imaging of biological tissues using nanospray desorption electrospray ionization mass spectrometry, Nat Protoc. 14 (2019) 3445–3470. https://doi.org/10.1038/s41596-019-0237-4.

[33] X. Li, R. Yin, H. Hu, Y. Li, X. Sun, S.K. Dey, J. Laskin, An integrated microfluidic probe for mass spectrometry imaging of biological samples, Angew. Chem., Int. Ed.59 (2020) 22388–22391. https://doi.org/10.1002/anie.202006531.

[34] X. Li, H. Hu, R. Yin, Y. Li, X. Sun, S.K. Dey, J. Laskin, High-throughput Nano-DESI mass spectrometry imaging of biological tissues using an integrated microfluidic probe, Anal Chem. 94 (2022) 9690–9696. https://doi.org/10.1021/acs.analchem.2c01093.

[35] M. Brouard, E. Halford, A. Lauer, C.S. Slater, B. Winter, W.H. Yuen, J.J. John, L. Hill, A. Nomerotski, A. Clark, J. Crooks, I. Sedgwick, R. Turchetta, J.W.L. Lee, C. Vallance, E. Wilman, The application of the fast, multi-hit, pixel imaging mass spectrometry sensor to spatial imaging mass spectrometry, Rev. Sci. Instrum. 83 (2012) 114101. https://doi.org/10.1063/1.4766938.

[36] J.H. Jungmann, L. MacAleese, R. Buijs, F. Giskes, A. de Snaijer, J. Visser, J. Visschers, M.J.J. Vrakking, R.M.A. Heeren, Fast, high resolution mass spectrometry imaging using a Medipix pixelated detector, J Am Soc Mass Spectrom. 21 (2010) 2023–2030. https://doi.org/10.1016/j.jasms.2010.08.014.

[37] J. Aoki, M. Toyoda, Development of novel projection-type imaging mass spectrometer, Rev. Sci. Instrum. 92 (2021) 053706. https://doi.org/10.1063/5.0037370.

[38] C. Vallance, M. Brouard, A. Lauer, C.S. Slater, E. Halford, B. Winter, S.J. King, J.W.L. Lee, D.E. Pooley, I. Sedgwick, R. Turchetta, A. Nomerotski, J.J. John, L. Hill, Fast sensors for time-of-flight imaging applications, Phys. Chem. Chem. Phys. 16 (2014) 383–395. https://doi.org/10.1039/c3cp53183j.

[39] J. Aoki, H. Hazamz, M. Toyoda, Novel ion extraction method for imaging mass spectrometry, J Mass Spectrom Soc Jpn. 59 (2011) 57–61. https://doi.org/10.5702/massspec.11-20.

[40] R.J. Burleigh, A. Guo, N. Smith, A. Green, S. Thompson, M. Burt, M. Brouard, Microscope imaging mass spectrometry with a reflectron, Rev. Sci. Instrum. 91 (2020) 23306. https://doi.org/10.1063/1.5142271.

[41] A. Körber, J.D. Keelor, B.S.R. Claes, R.M.A. Heeren, I.G.M. Anthony, Fast mass microscopy: Mass spectrometry imaging of a gigapixel image in 34 minutes, Anal Chem. 94 (2022) 14652–14658. https://doi.org/10.1021/acs.analchem.2c02870.

[42] M. Vestal, C. Vestal, S. Li, K. Parker, The seven S criteria for evaluating the performance of a MALDI mass spectrometer for MSI, J Am Soc Mass Spectrom. 31 (2020) 2521–2530. https://doi.org/10.1021/jasms.0c00216.

[43] J.M. Spraggins, K. v. Djambazova, E.S. Rivera, L.G. Migas, E.K. Neumann, A. Fuetterer, J. Suetering, N. Goedecke, A. Ly, R. van de Plas, R.M. Caprioli, High-performance molecular imaging with MALDI trapped ion-mobility time-of-flight (timsTOF) mass spectrometry, Anal Chem. 91 (2019) 14552–14560. https://doi.org/10.1021/acs.analchem.9b03612.

[44] A. v. Loboda, I. v. Chernushevich, A novel ion trap that enables high duty cycle and wide m/z range on an orthogonal injection TOF mass spectrometer, J Am Soc Mass Spectrom. 20 (2011) 1342–1348. https://doi.org/10.1016/J.JASMS.2009.03.018.

[45] P. Willis, J. Jaloszynski, V. Artaev, Improving duty cycle in the folded flight path high-resolution time-of-flight mass spectrometer, Int J Mass Spectrom. 459 (2021) 116467. https://doi.org/10.1016/j.ijms.2020.116467.

[46] K. DeLaney, A. Phetsanthad, L. Li, Advances in high-resolution MALDI mass spectrometry for neurobiology, Mass Spectrom Rev. 41 (2022) 194–214. https://doi.org/10.1002/mas.21661.

[47] A.P. Bowman, G.T. Blakney, C.L. Hendrickson, S.R. Ellis, R.M.A. Heeren, D.F. Smith, Ultra-high mass resolving power, mass accuracy, and dynamic range MALDI mass spectrometry imaging by 21-T FT-ICR MS, Anal Chem. 92 (2020) 3133–3142. https://doi.org/10.1021/acs.analchem.9b04768.

[48] G.W. Vandergrift, W. Kew, J.K. Lukowski, A. Bhattacharjee, A. v. Liyu, E.A. Shank, L. Paša-Tolić, V. Prabhakaran, C.R. Anderton, Imaging and direct sampling capabilities of nanospray desorption electrospray ionization with absorption-mode 21 tesla Fourier transform ion cyclotron resonance mass spectrometry, Anal Chem. 94 (2022) 3629–3636. https://doi.org/10.1021/acs.analchem.1c05216.

[49] P.C. Kooijman, K.O. Nagornov, A.N. Kozhinov, D.P.A. Kilgour, Y.O. Tsybin, R.M.A. Heeren, S.R. Ellis, Increased throughput and ultra-high mass resolution in DESI FT-ICR MS imaging through new-generation external data acquisition system and advanced data processing approaches, Sci Rep. 9 (2019). https://doi.org/10.1038/s41598-018-36957-1.

[50] Y.R. Xie, D.C. Castro, F. Lam, J. v. Sweedler, Accelerating Fourier transform-ion cyclotron resonance mass spectrometry imaging using a subspace approach, J Am Soc Mass Spectrom. 31 (2020) 2338–2347. https://doi.org/10.1021/jasms.0c00276.

[51] Y.R. Xie, D.C. Castro, S.S. Rubakhin, J. V. Sweedler, F. Lam, Enhancing the throughput of ft mass spectrometry imaging using joint compressed sensing and subspace modeling, Anal Chem. 94 (2022) 5335–5343. https://doi.org/10.1021/acs.analchem.1c05279.

[52] I. Lanekoff, K. Burnum-Johnson, M. Thomas, J. Short, J.P. Carson, J. Cha, S.K. Dey, P. Yang, M.C. Prieto Conaway, J. Laskin, High-speed tandem mass spectrometric in situ imaging by nanospray desorption electrospray ionization mass spectrometry, Anal Chem. 85 (2013) 9596–9603. https://doi.org/10.1021/AC401760S/SUPPL_FILE/AC401760S_SI_001.PDF.

[53] L. Lamont, G.B. Eijkel, E.A. Jones, B. Flinders, S.R. Ellis, T. Porta Siegel, R.M.A. Heeren, R.J. Vreeken, Targeted drug and metabolite imaging: Desorption electrospray ionization combined with triple quadrupole mass spectrometry, Anal Chem. 90 (2018) 13229–13235. https://doi.org/10.1021/acs.analchem.8b03857.

[54] C.G. Vasilopoulou, K. Sulek, A.D. Brunner, N.S. Meitei, U. Schweiger-Hufnagel, S.W. Meyer, A. Barsch, M. Mann, F. Meier, Trapped ion mobility spectrometry and PASEF enable in-depth lipidomics from minimal sample amounts, Nat Commun. 11 (2020) 311. https://doi.org/10.1038/s41467-019-14044-x.

[55] M. Colley, K.V. Djambazova, E.K. Neumann, A. Fuetterer, M. Krause, R.M. Caprioli, J.M. Spraggins, PASEF imaging mass spectrometry: High spatial resolution in situ molecular mapping and identification, in: 70th ASMS Conference, June 5-9, 2022, Minneapolis, Minnesota, n.d.

[56] A. Bartels, P. Dülk, D. Trede, T. Alexandrov, P. Maaß, Compressed sensing in imaging mass spectrometry, Inverse Probl. 29 (2013) 125015. https://doi.org/10.1088/0266-5611/29/12/125015.

[57] G.M.D.P. Godaliyadda, D.H. Ye, M.D. Uchic, M.A. Groeber, G.T. Buzzard, C.A. Bouman, A framework for dynamic image sampling based on supervised learning, IEEE Trans Comput Imaging. 4 (2017) 1–16. https://doi.org/10.1109/TCI.2017.2777482.

[58] F. Tang, Y. Bi, J. He, T. Li, Z. Abliz, X. Wang, Application of super-resolution reconstruction of sparse representation in mass spectrometry imaging, Rapid Commun. Mass Spectrom. 29 (2015)

1178–1184. https://doi.org/10.1002/RCM.7205.

[59] H. Hu, D. Helminiak, M. Yang, D. Unsihuay, R.T. Hilger, D.H. Ye, J. Laskin, High-throughput mass spectrometry imaging with dynamic sparse sampling, ACS Meas. Sci. Au. 2 (2022) 466–474. https://doi.org/10.1021/acsmeasuresciau.2c00031.

[60] M. Sandilya, S.R. Nirmala, Compressed sensing trends in magnetic resonance imaging, Eng. Sci. Technol. an Int. J. 20 (2017) 1342–1352. https://doi.org/10.1016/J.JESTCH.2017.07.001.

[61] M. Yousufi, M. Amir, U. Javed, M. Tayyib, S. Abdullah, H. Ullah, I.M. Qureshi, K.S. Alimgeer, M.W. Akram, K.B. Khan, Application of compressive sensing to ultrasound images: a review, Biomed Res Int. 2019 (2019). https://doi.org/10.1155/2019/7861651.

[62] J. Ke, L. Zhang, Q. Zhou, Applications of compressive sensing in optical imaging, Guangxue Xuebao/Acta Opt. Sin. 40 (2020). https://doi.org/10.3788/AOS202040.0111006.

[63] Y. Gao, L. Zhu, I. Norton, N.Y.R. Agar, A. Tannenbaum, Reconstruction and feature selection for desorption electrospray ionization mass spectroscopy imagery, J. Med. Imaging. 9036 (2014) 89–94. https://doi.org/10.1117/12.2043273.

[64] J.H. Rabe, D.A. Sammour, S. Schulz, B. Munteanu, M. Ott, K. Ochs, P. Hohenberger, A. Marx, M. Platten, C.A. Opitz, D.S. Ory, C. Hopf, Fourier transform infrared microscopy enables guidance of automated mass spectrometry imaging to predefined tissue morphologies, Sci Rep. 8 (2018) 1–11. https://doi.org/10.1038/s41598-017-18477-6.

[65] E.K. Neumann, K. v. Djambazova, R.M. Caprioli, J.M. Spraggins, Multimodal imaging mass spectrometry: Next generation molecular mapping in biology and medicine, J Am Soc Mass Spectrom. 31 (2020) 2401–2415. https://doi.org/10.1021/jasms.0c00232.

[66] D. Helminiak, H. Hu, J. Laskin, D.H. Ye, Deep learning approach for dynamic sparse sampling for high-throughput mass spectrometry imaging, Electron. Imaging. 2021 (2021) 1–7. https://doi.org/10.2352/ISSN.2470-1173.2021.15.COIMG-290.

[67] L.A. McDonnell, A. van Remoortere, R.J.M. van Zeijl, H. Dalebout, M.R. Bladergroen, A.M. Deelder, Automated imaging MS: Toward high throughput imaging mass spectrometry, J Proteomics. 73 (2010) 1279–1282. https://doi.org/10.1016/j.jprot.2009.10.011.